



Article

Functional and Structural Insights into the Human PPAR $\alpha/\delta/\gamma$ Targeting Preferences of Anti-NASH Investigational Drugs, Lanifibranor, Seladelpar, and Elafibranor

Shotaro Kamata ¹, Akihiro Honda ¹, Ryo Ishikawa ¹, Makoto Akahane ¹, Ayane Fujita ¹, Chihiro Kaneko ¹, Saeka Miyawaki ¹, Yuki Habu ¹, Yui Shiiyama ¹, Kie Uchii ¹, Yui Machida ¹, Takuji Oyama ² and Isao Ishii ^{1,*}

¹ Department of Health Chemistry, Showa Pharmaceutical University, Machida 194-8543, Tokyo, Japan

² Faculty of Life and Environmental Sciences, University of Yamanashi, Kofu 400-8510, Yamanashi, Japan

* Correspondence: i-ishii@ac.shoyaku.ac.jp

Abstract: No therapeutic drugs are currently available for nonalcoholic steatohepatitis (NASH) that progresses from nonalcoholic fatty liver via oxidative stress-involved pathways. Three cognate peroxisome proliferator-activated receptor (PPAR) subtypes (PPAR $\alpha/\delta/\gamma$) are considered as attractive targets. Although lanifibranor (PPAR $\alpha/\delta/\gamma$ pan agonist) and saroglitazar (PPAR α/γ dual agonist) are currently under investigation in clinical trials for NASH, the development of seladelpar (PPAR δ -selective agonist), elafibranor (PPAR α/δ dual agonist), and many other dual/pan agonists has been discontinued due to serious side effects or little/no efficacies. This study aimed to obtain functional and structural insights into the potency, efficacy, and selectivity against PPAR $\alpha/\delta/\gamma$ of three current and past anti-NASH investigational drugs: lanifibranor, seladelpar, and elafibranor. Ligand activities were evaluated by three assays to detect different facets of the PPAR activation: transactivation assay, coactivator recruitment assay, and thermal stability assay. Seven high-resolution cocrystal structures (namely, those of the PPAR $\alpha/\delta/\gamma$ -ligand-binding domain (LBD)-lanifibranor, PPAR $\alpha/\delta/\gamma$ -LBD-seladelpar, and PPAR α -LBD-elafibranor) were obtained through X-ray diffraction analyses, six of which represent the first deposit in the Protein Data Bank. Lanifibranor and seladelpar were found to bind to different regions of the PPAR $\alpha/\delta/\gamma$ -ligand-binding pockets and activated all PPAR subtypes with different potencies and efficacies in the three assays. In contrast, elafibranor induced transactivation and coactivator recruitment (not thermal stability) of all PPAR subtypes, but the PPAR δ/γ -LBD-elafibranor cocrystals were not obtained. These results illustrate the highly variable PPAR $\alpha/\delta/\gamma$ activation profiles and binding modes of these PPAR ligands that define their pharmacological actions.

Keywords: NAFLD; NASH; PPAR subtypes; dual/pan agonist; ligand-binding domain; X-ray crystallography



Citation: Kamata, S.; Honda, A.; Ishikawa, R.; Akahane, M.; Fujita, A.; Kaneko, C.; Miyawaki, S.; Habu, Y.; Shiiyama, Y.; Uchii, K.; et al. Functional and Structural Insights into the Human PPAR $\alpha/\delta/\gamma$ Targeting Preferences of Anti-NASH Investigational Drugs, Lanifibranor, Seladelpar, and Elafibranor.

Antioxidants **2023**, *12*, 1523. <https://doi.org/10.3390/antiox12081523>

Academic Editors: Greg Barritt and Eunus S. Ali

Received: 23 June 2023

Revised: 19 July 2023

Accepted: 27 July 2023

Published: 29 July 2023



Copyright: © 2023 by the authors. Licensee MDPI, Basel, Switzerland. This article is an open access article distributed under the terms and conditions of the Creative Commons Attribution (CC BY) license (<https://creativecommons.org/licenses/by/4.0/>).

1. Introduction

There is serious concern regarding the medical/economic burden of the treatment of the globally expanding number of patients with nonalcoholic fatty liver disease (NAFLD)/nonalcoholic steatohepatitis (NASH). NAFLD is defined by the evidence of hepatic steatosis (either through imaging or histology) and the absence of secondary causes of significant alcohol consumption, long-term use of a steatogenic medication, or monogenic hereditary disorders [1]. The overall prevalence of nonalcoholic fatty liver (NAFL) worldwide is estimated to be 32.4% [2], while an estimated 10–25% of NAFL patients progress to the development of NASH (a condition characterized by $\geq 5\%$ hepatic steatosis and inflammation with hepatic injury (e.g., ballooning) in the presence or absence of fibrosis [1]) in which oxidative stress plays a pivotal role by stimulating Kupffer cells, hepatic stellate cells, and hepatocytes [3]. NASH can further progress to cirrhosis, end-stage liver disease, or hepatocellular carcinoma [4], and NAFLD is the leading cause of liver-related morbidity

and mortality. NASH is the major cause of liver transplantation and, currently, there are no approved non-symptomatic therapies for NASH by the Food and Drug Administration (FDA) or the European Medicines Agency [5]. NASH is a multifaceted condition with variable coexisting metabolic complications such as obesity and type 2 diabetes, thereby further complicating its treatment [4]. Its therapeutic targets can be divided into four major categories: (i) metabolic targets, (ii) targets related to inflammation or cell injury, (iii) liver–gut axis targets, and (iv) targets related to fibrosis [5,6]. In this respect, the peroxisome proliferator-activated receptors (PPARs) are attractive therapeutic targets that could simultaneously improve steatosis, ballooning, inflammation, and fibrosis [6,7].

PPARs belong to the nuclear receptor superfamily and the ligand-activated transcription factors; they exist in three subtypes in mammals (namely, PPAR α , PPAR β/δ , and PPAR γ) with considerable amino acid identity (54–71% in humans). The synthetic PPAR α agonists known as “fibrates” have been widely used for the treatment of hypertriglyceridemia, while the synthetic PPAR γ agonists known as “thiazolidinediones (glitazones)” are anti-diabetic drugs. In the guidelines of the American Association for the Study of Liver Diseases, pioglitazone has been proposed for the treatment of biopsy-proven NASH. The PPAR pan agonist lanifibranor (IVA-337) and the PPAR α/γ dual agonist saroglitazar are currently in clinical trials for NASH (phase 3 in NCT04849728 and 2b in NCT05011305, respectively). However, the development of most glitazars (PPAR α/γ dual agonists), including muraglitazar, tesaglitazar, and aleglitazar, has been abandoned due to serious safety concerns [8]. The use of the PPAR δ -selective agonist seladelpar (MBX-8025) for the treatment of NASH has been once discontinued at phase 2b [9], while that of the PPAR α/δ dual agonist elafibranor against NASH has been discontinued due to its non-significant benefits [10]. Therefore, the risks and the benefits of each PPAR-targeting drug should be carefully discussed based on detailed analyses at molecular levels.

This study was designed so as to provide functional and structural insights into the potency, efficacy, and selectivity against PPAR $\alpha/\delta/\gamma$ of lanifibranor, seladelpar, and elafibranor. We have found that all three agents can activate all PPAR subtypes with highly different preferences in the three different PPAR activation assays undertaken herein. Furthermore, we have characterized the high-resolution structures of the PPAR $\alpha/\delta/\gamma$ -ligand-binding domain (LBD)–lanifibranor, the PPAR $\alpha/\delta/\gamma$ -LBD–seladelpar, and the PPAR α -LBD–elafibranor cocrystals through X-ray diffraction analyses.

2. Materials and Methods

2.1. PPAR Activation Assay 1: Transactivation Assay

In order to evaluate the PPAR $\alpha/\delta/\gamma$ -mediated transcriptional activation, pSG5-GAL–human PPAR $\alpha/\delta/\gamma$ chimera expression plasmids, a MH100(UAS) \times 4-tk-Luc reporter plasmid, and a pRL-CMV *Renilla* luciferase control plasmid under the control of a cytomegalovirus promoter were cotransfected into COS-7 cells (No. RCB0539; Riken BRC Cell Bank, Tsukuba, Ibaraki, Japan) that were maintained in Dulbecco’s modified Eagle’s medium (DMEM) supplemented with 10% fetal bovine serum (FBS) and antibiotics, at 37 °C, in a 5% CO₂/95% air incubator. The pSG5-GAL–hPPAR $\alpha/\delta/\gamma$ plasmids express fusion proteins comprising the yeast transcription factor GAL4 DNA-binding domain and each of the human PPAR $\alpha/\delta/\gamma$ -LBDs [11,12]. The MH100(UAS) \times 4-tk-Luc plasmid contains four copies of the MH100 GAL4 binding site and the *Firefly* luciferase gene [13]. The cells were transfected with those plasmids and were treated with various PPAR ligands, and both *Firefly* and *Renilla* luciferase activities were measured using the Dual-Glo Luciferase Assay System (Promega, Madison, WI, USA) as described previously [14]. The transactivation activities were expressed as percentages of the maximal *Firefly* luciferase responses induced by potent/specific PPAR $\alpha/\delta/\gamma$ agonists: GW7647 (1 μ M) for PPAR α , GW501516 (0.02 μ M) for PPAR δ , and GW1929 (1 μ M) for PPAR γ [14], after normalization with the *Renilla* luciferase responses. GW7647, GW501516, and pioglitazone were purchased from the Cayman Chemical Company (Ann Arbor, MI, USA). Elafibranor, lanifi-

branor, seladelpar, and saroglitazar were purchased from ChemScene (Monmouth Junction, NJ, USA). GW1929 was purchased from Sigma-Aldrich (St. Louis, MO, USA).

2.2. Recombinant PPAR α / δ / γ -LBD Expression and Purification

Human PPAR α -LBD (amino acids 200–468), PPAR δ -LBD (amino acids 170–441), and PPAR γ -LBD (amino acids 203–477 in isoform 1) were expressed as amino-terminal His-tagged proteins by the pET28a vector (Novagen, Madison, WI, USA) in Rosetta (DE3) pLysS competent cells (Novagen) and were subsequently purified using three-step chromatography, as previously described in detail [14–17].

2.3. PPAR Activation Assay 2: PGC1 α /SRC1 Coactivator Recruitment Assay

The activation status of each PPAR α / δ / γ subtype was also determined by a time-resolved fluorescence resonance energy transfer (TR-FRET) assay that detects physical interactions between His-tagged hPPAR α / δ / γ -LBD proteins and a biotin-labeled PPAR γ coactivator 1 α (PGC1 α) coactivator peptide (biotin-EAEEPSLLKLLLAPANTQ (amino acids 137–155) synthesized by GenScript) or a steroid receptor coactivator 1 (SRC1) peptide (biotin-CPSSHSLTERHKILHRLLLQEGSPS (amino acids 676–700) from GenScript) using the LANCE Ultra TR-FRET assay (PerkinElmer, Waltham, MA, USA) [14,15,17]. A 9.5 μ L aliquot of PPAR α / δ / γ -LBD (400 nM in buffer A consisting of 10 mM HEPES-NaOH (pH 7.4), 150 mM NaCl, 0.005% Tween 20, and 0.1% fatty acid-free bovine serum albumin (BSA) for PPAR α / γ -LBD; 400 nM in buffer B consisting of 50 mM HEPES-NaOH (pH 7.4), 50 mM KCl, 1 mM EDTA, 0.5 mM dithiothreitol, and 0.1% fatty acid-free BSA for PPAR δ -LBD), 0.5 μ L of a 100 \times ligand solution (in DMSO), and 5 μ L of biotin-PGC1 α (4 μ M) or biotin-SRC1 peptide (8 μ M) were mixed in a well of Corning 384-well low-volume, white, round-bottom, polystyrene non-binding surface microplate. Subsequently, 5 μ L of 4 nM Eu-W1024-labeled anti-6 \times His antibody/80 nM ULight-Streptavidin (PerkinElmer) was added to each well, and the microplate was incubated in the dark for 2 h, at room temperature. FRET signals were detected at one excitation filter (340/12) and at two emission filters (615/12 and 665/12) using a Varioskan Flash double monochromator microplate reader (Thermo Fisher Scientific, Waltham, MA, USA). The parameters for the measurements at 615 and 665 nm were an integration time of 200 μ s and a delay time of 100 μ s. The 665 nm emissions were due to ULight-FRET, while the 615 nm emissions were due to Eu-W1024. The 665/615 ratio was calculated and normalized to the negative control reaction using 1% DMSO. The nonlinear fitting and the calculation of the EC₅₀ were performed using the Prism 9 software (GraphPad, San Diego, CA, USA).

2.4. PPAR Activation Assay 3: Thermal Stability Assay Using Circular Dichroism Spectroscopy

PPAR α / δ / γ -LBD proteins (10 μ M) were incubated with different concentrations of ligands in buffer C consisting of 20 mM Tris-HCl (pH 8.0), 150 mM NaCl, 1 mM Tris 2-carboxyethylphosphine (TCEP)-HCl, and 10% glycerol. The circular dichroism (CD) spectra were monitored within a 200–260 nm range at increasing temperatures from 30 $^{\circ}$ C to 70 $^{\circ}$ C (2 $^{\circ}$ C/min) using a J-1500 spectropolarimeter equipped with a PTC-510 thermal controller (JASCO, Tokyo, Japan). The spectra of all PPARs displayed local minima at 208 and 222 nm, which is a typical feature of α -helical proteins [18]. The thermal stability of the PPARs was investigated by continuously monitoring the ellipticity changes at 222 nm during the thermal denaturation [14,15], and a single-site sigmoidal dose–response curve fitting program (Prism 9) was used in order to obtain the melting temperature (T_m) that corresponds to the midpoint of the denaturation process. The ligand-induced increases in the T_m values were defined as ΔT_m .

2.5. Cocrystallization of PPAR α / δ / γ -LBD with Lanifibranor, Seladelpar, or Elafibranor

2.5.1. PPAR α Cocrystals

We have previously obtained the PPAR α -LBD–clofibric acid (a low affinity PPAR α ligand and with an EC₅₀ value of 574 μ M in the PGC1 α recruitment activity) [15]–SRC1 (LTERHK-

ILHRLQEG; (amino acids 683–697) from GenScript, Piscataway, NJ, USA) cocrystal by cocrystallization with delipidized PPAR α [16], and have revealed its high-resolution (2.09-Å) structure (PDB ID: 7BPY) [15]. The PPAR α -LBD–clofibric acid–SRC1 cocrystals were soaked in a reservoir solution (0.1 M HEPES (pH 7.5)/20% PEG3350) containing 2 mM of lanifibranor or elafibranor (final 10% DMSO) at 4 °C, for three days, in order to obtain cocrystals with each ligand. The cocrystallization with seladelpar was performed in hanging-drop mixtures of 0.5 μ L PPAR α -LBD (20 mg/mL in buffer C), 0.5 μ L ligand (2 mM in buffer C), and 1 μ L reservoir solution (0.1 M Tris (pH 8.5)/25% PEG3350), at 4 °C, for several weeks.

2.5.2. PPAR δ Cocrystals

The cocrystallization of PPAR δ -LBD–lanifibranor/seladelpar was performed in hanging-drop mixtures of 0.5 μ L of PPAR δ -LBD (10 mg/mL in buffer C), 0.1 μ L of 10 mM ligand, 0.3 μ L of buffer D (20 mM Tris-HCl (pH 8.0), 500 mM ammonium acetate, 1 mM TCEP-HCl, and 10% glycerol), 0.1 μ L of 5% *n*-octyl- β -D-glucoside, and 1 μ L reservoir solution (50 mM Bis-Tris propane (pH 7.5), 14% PEG8000, 0.2 M KCl, 6% propanediol, 1 mM EDTA, 1 mM CaCl₂ for PPAR δ -LBD–lanifibranor; 50 mM Bis-Tris propane (pH 8.0), 14% PEG8000, 0.1 M KSCN, 6% propanediol, 1 mM EDTA, 1 mM CaCl₂ for PPAR δ -LBD–seladelpar), at 20 °C, for several weeks.

2.5.3. PPAR γ Cocrystals

The cocrystallization of PPAR γ -LBD–lanifibranor/seladelpar–SRC1 was performed in hanging-drop mixtures of 0.5 μ L PPAR γ -LBD (20 mg/mL in buffer C), 0.5 μ L ligand (2 mM in buffer C), and 1 μ L reservoir solution (0.1 M HEPES-NaOH (pH 7.5)/1.0 M trisodium citrate dihydrate for PPAR γ -LBD–lanifibranor–SRC1; 0.1 M Tris (pH 8.0)/1.1 M trisodium citrate dihydrate for PPAR γ -LBD–seladelpar–SRC1), at 20 °C, for several weeks.

All obtained cocrystals were briefly soaked in a cryoprotection buffer (each reservoir solution plus 20% glycerol for PPAR α / δ -LBD crystals and 30% glycerol for PPAR γ -LBD crystals). Subsequently, these were flash-cooled in a stream of liquid nitrogen until the X-ray diffraction analysis was conducted.

2.6. X-ray Diffraction: Data Collection and Model Refinement

Datasets were collected by a BL-5A or a BL-17A beamline at the Photon Factory (Tsukuba, Ibaraki, Japan) using synchrotron radiation of 1.0 Å. Diffraction data were collected at a 0.1° oscillation per frame, and a total of 1800 frames (180°) were recorded for a 1.0-Å X-ray crystallography [14,15,17]. Data processing and scaling were carried out using the XDS X-ray detector software (version February 5, 2021) [19] and AIMLESS (version 0.5.21) [20], respectively. Resolution cutoff values ($R_{\text{merge}} < 0.5$, $R_{\text{pim}} < 0.3$, and completeness > 0.9) were set by the highest resolution shell [14,15,17]. All structures were determined by using the molecular replacement in PHASER (version 2.7.16) [21] with Protein Data Bank (PDB) IDs: 3SP6 for PPAR α -LBD, 2ZLN or 7WGL for PPAR δ -LBD, and 1WM0 or 7WGO for all PPAR γ -LBDs as the search model. Refinement was performed using the iterative cycles of the model adjustment in two programs: COOT (version 0.8.2) [22] and PHENIX (version 1.11.1-2575-000) [23]. The structures were constructed using the PyMOL program (version 2.5.0). All collection data and refinement statistics are summarized in Supplementary Materials Table S1.

2.7. Evaluation of Molecular Interactions between PPAR-LBD Amino Acids and Ligands

Based on those X-ray cocrystal structures, proximity distances between each amino acid in PPAR α / δ / γ -LBD and the three ligands were measured using PyMOL. All PPAR α / δ / γ -LBD amino acids that have 4.5 Å or less proximity distances from the ligands were listed in Table S2. All molecular interactions between those amino acids and the ligands were evaluated with the MolDock scores using Ligand Energy Inspector programs in Molegro Virtual Docker (MVD) software (version 6.0; CLC bio, Aarhus, Denmark) (Table S2). The scoring function of

MolDock is based on an extended piecewise linear potential including new hydrogen bonding and electrostatic terms.

3. Results

3.1. Transactivation of Gene Expression via PPAR α / δ / γ -LBD

For the undertaking of the comparison of the potency, efficacy, and selectivity of the five PPAR ligands (Figure 1A) against the PPAR subtypes, we evaluated their PPAR α / δ / γ activation using three different methods: a cell-based transactivation assay, a coactivator recruitment assay, and a thermal stability assay, as we previously performed on three fibrates (namely, bezafibrate, fenofibric acid, and pemafibrate) [14]. The cell-based transactivation assay utilizing the Gal4–PPAR-LBD system is the most widely used method for the determination of PPAR activation by certain ligands, although their responses depend on the used cell types in which several coactivators with altered functions are differentially expressed [24–26]. The maximal effects of the PPAR-selective full agonists (1 μ M GW7647 for PPAR α , 0.02 μ M GW501516 for PPAR δ , and 1 μ M GW1929 for PPAR γ) [14] in COS-7 cells were considered as the 100% transactivation responses. The “so-called” PPAR pan agonist lanifibranor [27] indeed activated all PPAR subtypes with EC₅₀ values of 398 nM (for δ) < 572 nM (for γ) < 4.66 μ M (for α), and equivalent efficacies (13.3% of the maximal responses for α / δ and 24.9% for γ) (Figure 1B). The PPAR δ -selective agonist seladelpar [28] activated PPAR δ with the highest potency (EC₅₀: 20.2 nM) and efficacy (99.3%) compared to PPAR α (1.64 μ M and 41.0%) and PPAR γ (3.53 μ M and 58.5%) (Figure 1C). Unexpectedly, the PPAR α / δ dual agonist elafibranor [29] activated all PPAR subtypes with potencies (EC₅₀) of 388 nM (for α) < 2.12 μ M (for γ) < 3.13 μ M (for δ) and efficacies of 38.5% (for α / γ) > 14.8% (for δ), thereby acting like a PPAR α / γ dual agonist (Figure 1D). In contrast, the genuine PPAR α / γ dual agonist saroglitazar [17] activated the PPAR α / γ at higher potencies (190 nM/311 nM vs. > 10 μ M in δ) and efficacies (56.4%/89.4% vs. 6.0% in δ) (Figure 1E). The PPAR γ -selective full agonist pioglitazone [30] indeed activated PPAR γ with the highest potency (EC₅₀: 479 nM) and efficacy (104%) compared to PPAR α (4.79 μ M and 25.2%) and PPAR δ (>20 μ M and 0.518%) (Figure 1F). These findings reveal that four of the five assessed PPAR ligands (i.e., except for elafibranor) act much as expected.

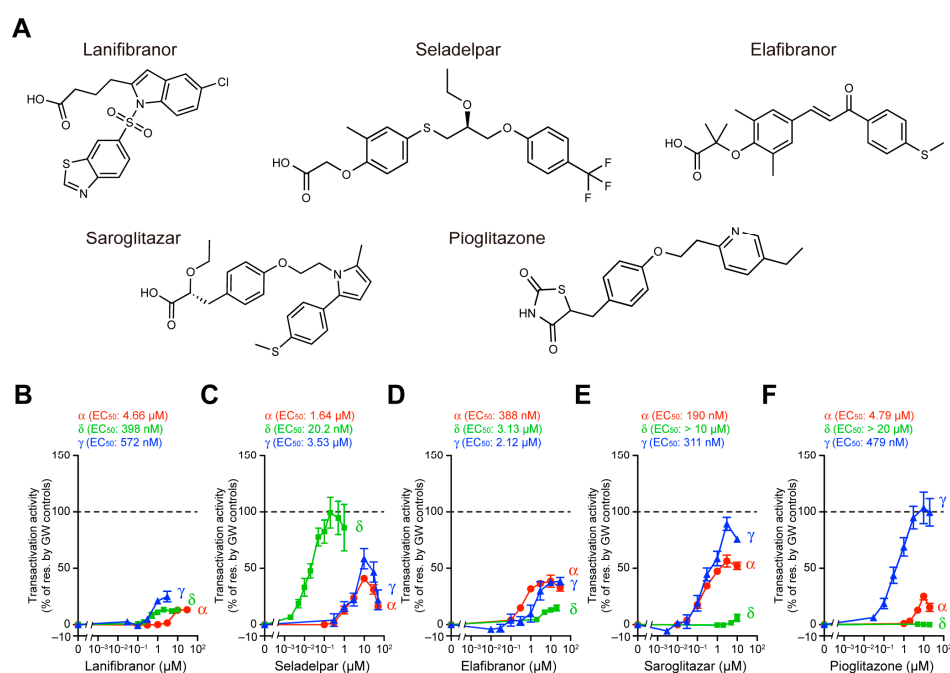


Figure 1. LBD-mediated human PPAR α / δ / γ transactivation by PPAR ligands. (A) Chemical structures of the five PPAR ligands used in this study. (B–F) LBD-mediated PPAR α / δ / γ transactivation

was induced in COS-7 cells by PPAR α -selective GW7647, PPAR δ -selective GW501516, and PPAR γ -selective GW1929 in a concentration-dependent manner, and their maximal responses (at 1, 0.02, and 1 μ M, respectively) were considered as 100% (dashed lines) of the responses. Concentration-dependent relative transactivation activities by lanifibranor (**B**), seladelpar (**C**), elafibranor (**D**), saroglitazar (**E**), and pioglitazone (**F**) are shown as percent responses with calculated EC₅₀ values. Data are presented as the mean \pm standard error (SE) of three independent experiments with duplicate samples.

3.2. PGC1 α /SRC1 Coactivator Recruitment via PPAR α / δ / γ -LBD

The ligand-bound activated forms of PPARs are stabilized by associations with specific coactivators, thereby enabling the regulation of specific gene expression [24,26]. The different coactivator recruitment profiles via PPAR γ -LBD were observed for rosiglitazone and lanifibranor [31]. The TR-FRET-based detection of the physical association between PPAR α / δ / γ -LBD and their coactivators is a highly sensitive cell-free assay for evaluating the activities of PPAR ligands [14]. Again, the maximal effects exerted by the PPAR-selective full agonists (1 μ M GW7647, GW501516, and GW1929) [14] for two types of coactivator peptides (PGC1 α and SRC1) that have altered functions in terms of energy expenditure [25] were considered as the 100% recruitment responses [14]. Lanifibranor recruited both PGC1 α and SRC1 to all PPAR α / δ / γ -LBD structures with equivalent potencies but altered efficacies: $\gamma > \delta > \alpha$ in the case of PGC1 α (Figure 2A) and $\alpha \sim \delta \sim \gamma$ in the case of SRC1 (Figure 2B). Seladelpar recruited both PGC1 α and SRC1 to PPAR δ -LBD with the highest potencies (30.7 nM and 111 nM, respectively) and efficacies (124% and 83.0%, respectively) compared to those of their recruitment to PPAR α / γ -LBD (Figure 2C,D). It should be noted that seladelpar recruited PGC1 α but not SRC1 to PPAR γ -LBD (Figure 2C,D). Although elafibranor recruited PGC1 α to all PPAR α / δ / γ -LBD structures with similar potencies and efficacies (Figure 2E), it recruited SRC1 with a higher potency and efficacy to PPAR α -LBD (4.95 μ M and 59.2%) than to PPAR δ / γ -LBD (Figure 2F). Saroglitazar recruited both PGC1 α and SRC1 to PPAR α / γ -LBD, but not to PPAR δ -LBD (Figure 2G,H), while pioglitazone recruited both PGC1 α and SRC1 to PPAR γ -LBD, but not to PPAR α / δ -LBD (only slightly to PPAR α -LBD in the case of SRC1) (Figure 2I,J). Those recruitment profiles were found to be almost identical to their transactivation profiles, although each PPAR ligand displayed different activities toward PGC1 α and SRC1.

3.3. Thermal Stability of PPAR α / δ / γ -LBD

Nuclear receptors, including PPARs, display an increased thermal stability upon ligand binding, which is detectable through CD spectroscopy [32]. Ligand-induced alterations in the T_m values at 222 nm are considered as the reflection of stable α -helical structures in PPARs, because ligand binding stabilizes the ligand-binding portion (LBP) [33]. The basal (only solvent; 0.1% DMSO) T_m values were 49.54 $^{\circ}$ C \pm 0.12 $^{\circ}$ C ($n = 4$), 51.76 $^{\circ}$ C \pm 0.17 $^{\circ}$ C ($n = 6$), and 48.95 $^{\circ}$ C \pm 0.16 $^{\circ}$ C ($n = 4$) for PPAR α / δ / γ -LBD, respectively. The PPAR α / δ / γ -selective GW compounds (GW7647, GW501516, and GW1929, respectively) indeed exhibited highly increased T_m values with their highest soluble (in 0.1% DMSO) concentrations (10, 50, and 10 μ M, respectively) so as to match the 10 μ M PPAR α / δ / γ -LBD protein in the assay mixture (Figure 3A). Lanifibranor increased the T_m values in all PPAR α / δ / γ -LBD complexes, with the highest values being evident in PPAR γ -LBD (61.4%) (Figure 3A,B), which is similar to its effect upon the PGC1 α recruitment (Figure 2A). Seladelpar also increased the T_m values in all PPAR α / δ / γ -LBD complexes with the highest values being evident in PPAR δ -LBD (Figure 3C), which is similar to all other assays (Figures 1C and 2C,D). In contrast, elafibranor did not significantly alter the T_m values in the PPAR α / δ / γ -LBD complexes (Figure 3D). Saroglitazar highly increased the T_m values in all PPAR α / δ / γ -LBD complexes, with the highest values being evident in PPAR γ -LBD and then in PPAR α -LBD (Figure 3E), whereas pioglitazone increased the T_m values only slightly in the case of PPAR γ -LBD and exerted no effects upon PPAR α / δ -LBD (Figure 3F). The thermal stability experiments illustrated other facets of the PPAR activation by those ligands.

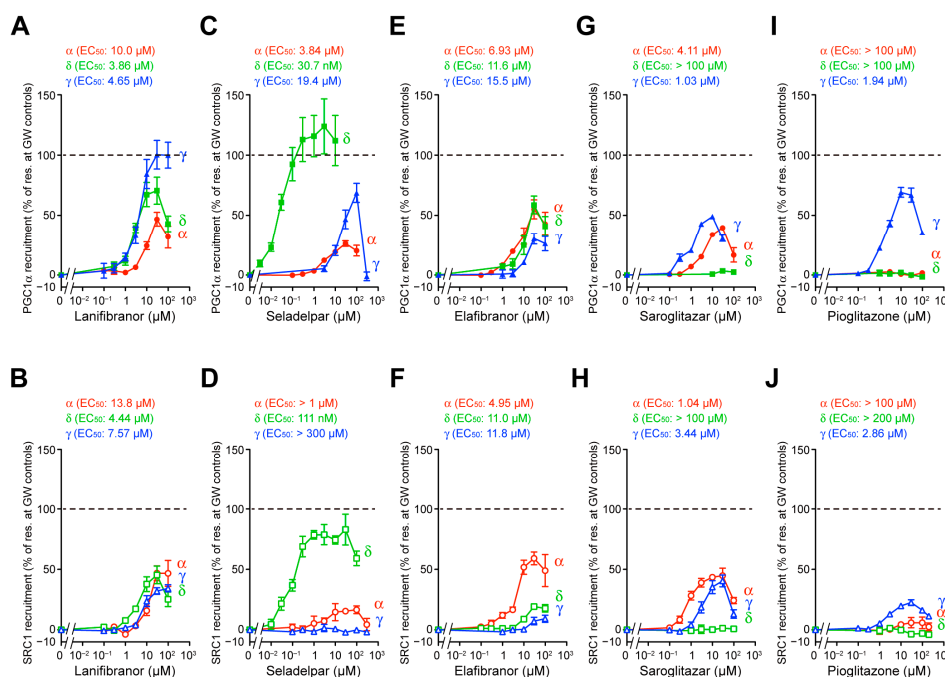


Figure 2. TR-FRET-based LBD-mediated human PPAR α / δ / γ coactivator recruitment assay. The LBD-mediated PPAR α / δ / γ recruitment of coactivator peptides, PGC1 α and SRC1, was induced by PPAR α -selective GW7647, PPAR δ -selective GW501516, and PPAR γ -selective GW1929 in a concentration-dependent manner, and their maximal responses (all at 1 μ M) were considered as the 100% responses (dashed lines). The PGC1 α (A,C,E,G,I) or the SRC1 (B,D,F,H,J) recruitment activities by lanifibranor (A,B), seladelpar (C,D), elafibranor (E,F), saroglitazar (G,H), and pioglitazone (I,J) were investigated. Data are presented as the mean \pm SE of three or four independent experiments with duplicate samples, and the calculated EC₅₀ values are shown.

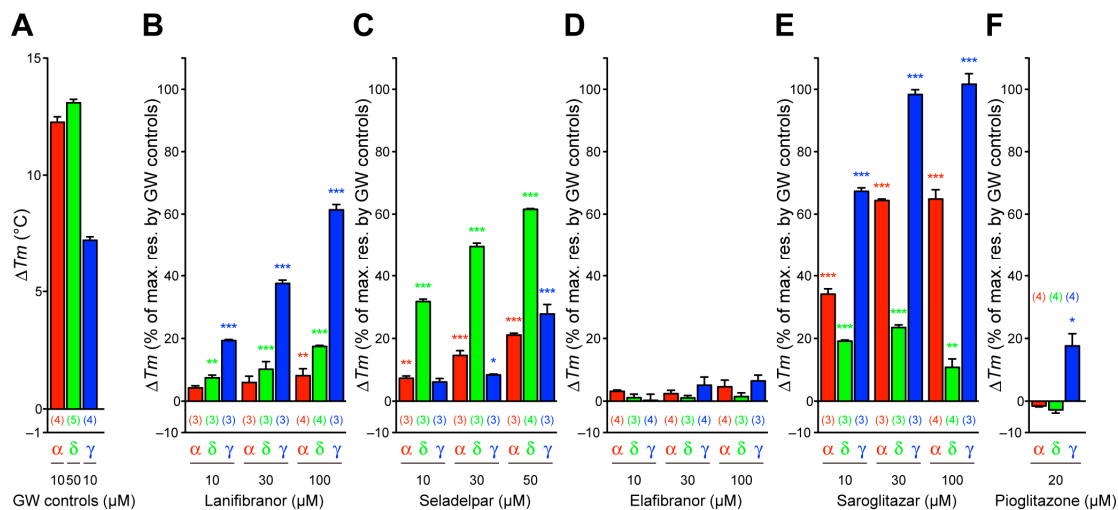


Figure 3. Circular dichroism-based PPAR α / δ / γ -LBD thermal stability assay. The PPAR α / δ / γ -LBD exhibited increased T_m values (ΔT_m) at 222 nm after an exposure to PPAR α -selective GW7647, PPAR δ -selective GW501516, and PPAR γ -selective GW1929 at their highest soluble concentrations (10, 50, and 10 μ M, respectively) (A) that were considered as the maximal (100%) responses. Relative ΔT_m responses by lanifibranor (B), seladelpar (C), elafibranor (D), saroglitazar (E), and pioglitazone (F) were measured as the reflection of the thermal stability of the α -helical structures in the PPAR α / δ / γ -LBD. Data are presented as the mean \pm SE of three or four (in parentheses) independent experiments. Differences vs. basal levels (with 0.1% DMSO) were statistically assessed by one-way ANOVA, followed by a Dunnett’s post hoc test: * $p < 0.05$, ** $p < 0.01$, and *** $p < 0.001$.

3.4. Structures of the PPAR α / δ / γ -LBD–Lanifibranor Complexes

After some trial and error using various cocrystallization techniques that we applied for PPAR α -LBD and its numerous ligands [15], including conventional cocrystallization with multiple buffer sets, cross-seeding, soaking, coactivator addition, and delipidation in order to remove endogenous fatty acids [16], the PPAR α -LBD–lanifibranor cocrystals were obtained by soaking the PPAR α -LBD–clofibrac acid–SRC1 cocrystals [16] in a buffer containing lanifibranor (Figure S1A). X-ray diffraction analyses revealed their dimeric structures (PDB ID: 8HUK): one holding a single lanifibranor molecule between H3 and H7, but not the SRC1 peptide (Figure 4A,B), and another with SRC1, but not with lanifibranor (Figure S2A,B). The dimeric structure of the PPAR δ -LBD–lanifibranor cocrystals (Figure S1B) was obtained using cocrystallization without coactivators (PDB ID: 8HUL), as both have a single lanifibranor molecule in the same position (Figures 4D,E and S2C,D). The monomeric structure of PPAR γ -LBD–lanifibranor cocrystals (Figure S1C) was obtained using cocrystallization with SRC1 (PDB ID: 8HUM) (Figure 4G,H). The structures of lanifibranor bound to PPAR α / δ / γ -LBD were solved in a monoclinic space group $P2_1$ at a 2.98 Å resolution, a monoclinic space group $P2_1$ at a 2.46 Å resolution, and an orthorhombic space group $P2_12_12_1$ at a 2.29 Å resolution (Table S1). Obtained structures were identical to previously reported active conformations [14,15,17] that form the Activation Function-2 (AF-2) helix 12, thereby providing root mean square distances of 0.60 Å (226 common C α positions in PPAR α / δ) and 0.53 Å (212 common C α positions in PPAR α / γ) (Figure 4A,D,G).

The carboxylic groups of the PPAR ligands are known to stabilize the AF-2 helix 12 through hydrogen bonds (red dotted lines) and electrostatic interactions (blue dotted lines) with the four surrounding consensus amino acids [14]: Ser280/Tyr314/His440/Tyr464 in PPAR α -LBD (Figure 4C), Thr253/His287/His413/Tyr437 in PPAR δ -LBD (Figure 4F), and Ser289/His323/His449/Tyr473 in PPAR γ -LBD (Figure 4I). However, a very close (2.3-Å) proximity was observed in the case of Y473 of PPAR γ and lanifibranor (Figure 4I). We have previously defined five regions in PPAR α -LBP (Arms I–III/X and Center) [15] and four regions (Arms II/III/X and Center) in PPAR δ / γ -LBP [14]. Lanifibranor was found to locate in the same position of the Center region in PPAR α / δ / γ -LBD, although its benzothiazole moiety in PPAR δ was flipped sideways when compared to that in PPAR α / γ (Figure 4J). A previous cocrystallization study [31] located lanifibranor in the “Center” (for its benzothiazole ring), the “Arm II” (for its 5-chloroindole moiety), and the “Arm III” (for its carboxylic moiety) regions (yellow in Figure 4K); however, in this study, no electron density was observed in the “Arm III” region (Figure 4K). Our structure seems more reasonable because the interaction of the carboxylic groups of lanifibranor with the four consensus amino acids contributes to the stabilization of the AF-2 helix 12 so as to facilitate the recruitment of coactivators in all PPAR subtypes.

3.5. Structures of the PPAR α / δ / γ -LBD–Seladelpar Complexes

Due to the fact that seladelpar is a relatively low-affinity PPAR α / γ ligand (Figures 1C, 2C,D and 3C), its cocrystals were obtained by cocrystallization with a delipidized PPAR α -LBD [15] or with PPAR γ -LBD and SRC1 (Figure S1D,F). In contrast, the PPAR δ -LBD–seladelpar cocrystals were obtained by employing cocrystallization without coactivators (Figure S1E). X-ray diffraction has revealed the monomeric structures for PPAR α (Figure 5A,B) and PPAR γ (Figure 5G,H), as well as the dimeric structure for PPAR δ (Figures 5D,E and S2E,F). The structures of seladelpar bound to PPAR α / δ / γ -LBD were solved in a monoclinic space group $P2_1$ at a 2.01 Å resolution (PDB ID: 8HUN), a monoclinic space group $P2_1$ at a 2.67 Å resolution (PDB ID: 8HUO), and an orthorhombic space group $P2_12_12_1$ at a 2.36 Å resolution (PDB ID: 8HUP), respectively (Table S1). The electron density maps located a single seladelpar molecule per PPAR α / δ / γ -LBD protein monomer (Figures 5B,E,H, and S2F). Seladelpar was located in the similar positions of the asymmetric units (Figures 5B and S2F). The obtained PPAR α / δ / γ -LBD helical structures were identical to those of previously reported active conformations described for lanifibranor above. Seladelpar was found to be located in the similar position of the “Center” and

the “Arm II” regions in PPAR α / δ / γ -LBD; however, its orientations differed (Figure 5J). Likewise, the orientations of the carboxylic group of seladelpar toward the four consensus amino acids in PPAR α / δ / γ -LBD (Figure 5C,F,I) were different from those of lanifibranor (Figure 4C,F,I). The loss of the interaction with His323/His449/Tyr473 in PPAR γ (Figure 5I) might explain the weak activity of seladelpar against PPAR γ .

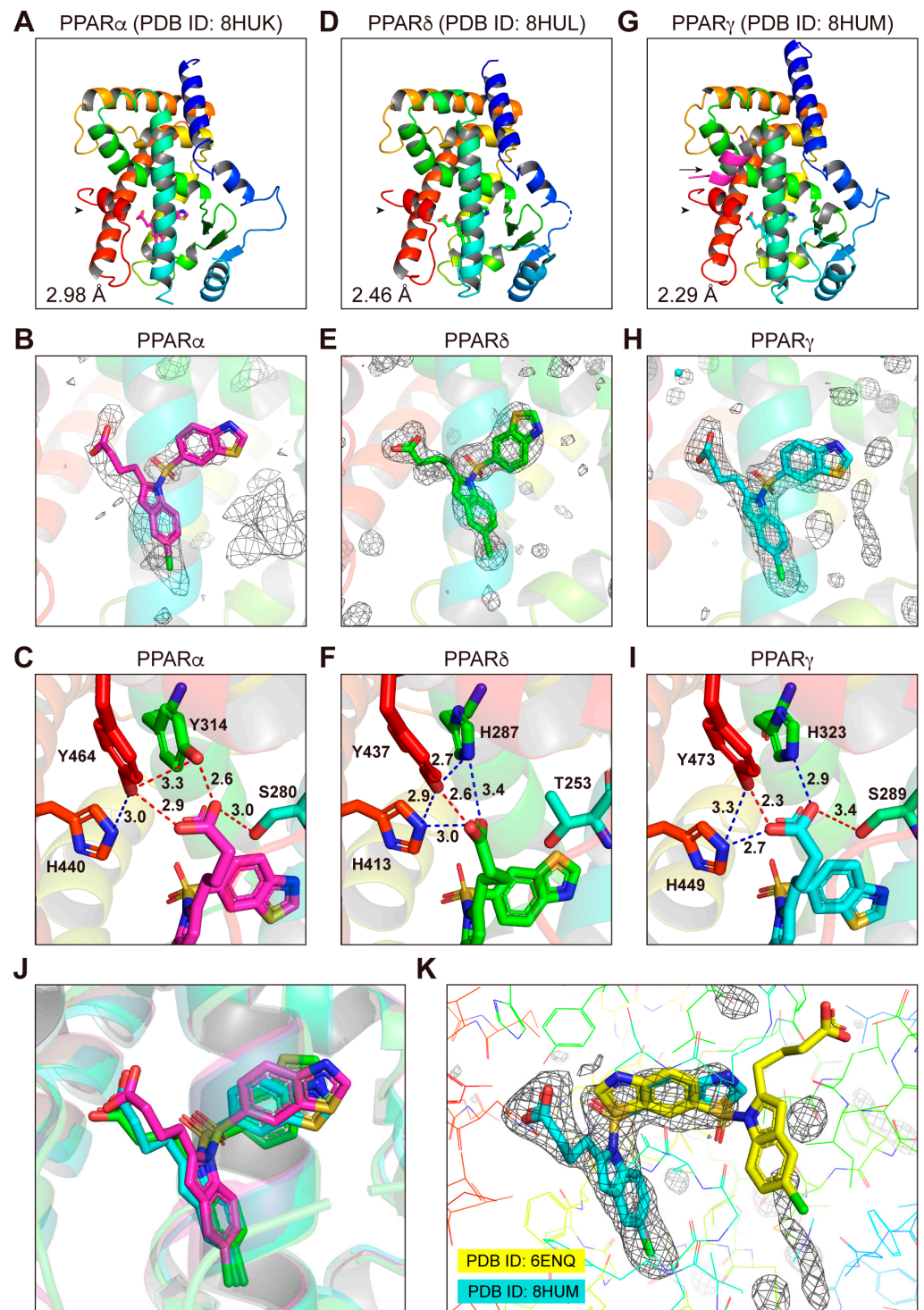


Figure 4. PPAR α / δ / γ -LBD–lanifibranor cocrystal structures. Cocrystals of lanifibranor and PPAR α -LBD (A–C), PPAR δ -LBD (D–F), or PPAR γ -LBD (G–I) were analyzed using X-ray diffraction. (A,D,G) Overall

structures of the complexes deposited in PDB with IDs: 8HUK, 8HUL, and 8HUM, respectively. The SRC1 peptide (α -helix in magenta) and the AF-2 helix 12 (α -helix in red) are indicated by arrows (only in (G)) and arrowheads, respectively. The highest resolutions are labeled. (B,E,H) Magnified views of lanifibranor located in the “Center” region of PPAR α / δ / γ -LBD. The electron density is shown in the mesh via F_o-F_c omit maps contoured at $+3.0\sigma$. A water molecule is presented as a cyan sphere in (H). (C,F,I) Hydrogen bonds and electrostatic interactions between lanifibranor and the four consensus amino acid residues (that recognize the carboxyl moiety of lanifibranor) are indicated by red and blue dotted lines, respectively, along with their distances (in Å). (J) Superposed view of lanifibranor in PPAR α (magenta)/PPAR δ (green)/PPAR γ (cyan)-LBD cocrystal structures. (K) Superposed view of our F_o-F_c omit maps of PPAR γ -LBD–lanifibranor (the same with (H)) and lanifibranor in a previous PDB submission (ID: 6ENQ).

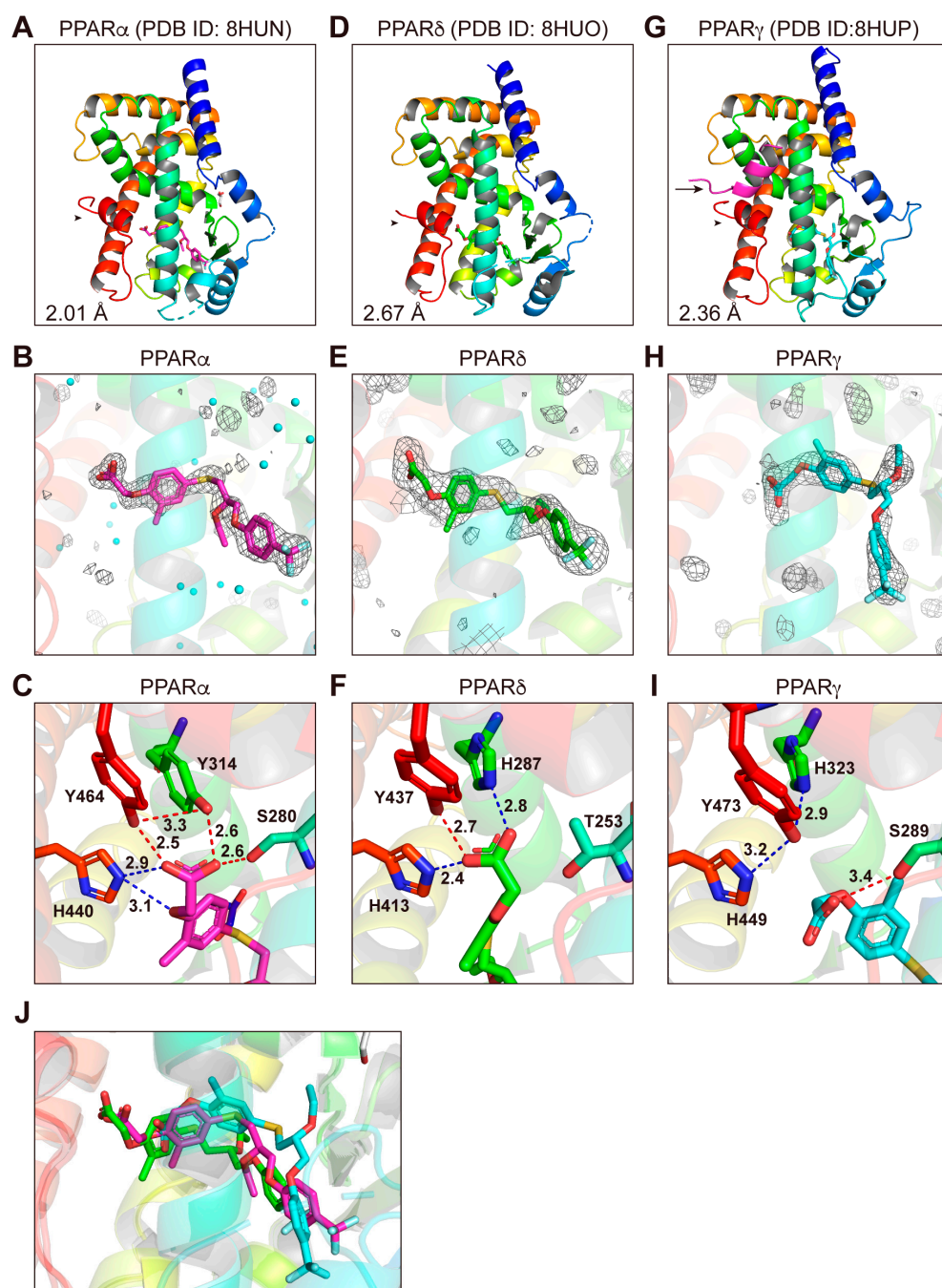


Figure 5. PPAR α / δ / γ -LBD–seladelpar cocrystal structures. Cocrystals of seladelpar and PPAR α -LBD

(A–C), PPAR δ -LBD (D–F), or PPAR γ -LBD (G–I) were analyzed using X-ray diffraction. (A,D,G) Overall structures of the complexes deposited in PDB with IDs 8HUN, 8HUO, and 8HUP, respectively. The SRC1 peptide (α -helix in magenta) and the AF-2 helix 12 (α -helix in red) are indicated by arrows (only in (G)) and arrowheads, respectively. The highest resolutions are labeled. (B,E,H) Magnified views of seladelpar located in the “Center” and the “Arm II” regions of PPAR $\alpha/\delta/\gamma$ -LBD. The electron density is shown in the mesh via F_o-F_c omit maps contoured at $+3.0\sigma$. Water molecules are presented as cyan spheres in (B). (C,F,I) Hydrogen bonds and electrostatic interactions between seladelpar and the four consensus amino acid residues (that recognize the carboxyl moiety of seladelpar) are indicated by red and blue dotted lines, respectively, along with their distances (in Å). (J) Superposed view of seladelpar in PPAR α (magenta)/PPAR δ (green)/PPAR γ (cyan)-LBD cocrystal structures.

3.6. Structures of the PPAR α -LBD–Elafibranor Complex

The PPAR α -LBD–elafibranor cocrystals were obtained by soaking the PPAR α -LBD–clofibric acid–SRC1 cocrystals [15] in a buffer containing elafibranor (Figure S1G). X-ray diffraction analyses revealed the monomeric structure with a single elafibranor and SRC1 (Figure 6A,B). The complex structure was solved in a monoclinic space group $P2_1$ at a 1.65 Å resolution (Table S1; PDB ID: 8HUQ). The obtained structures were identical to the previously reported active conformations described above, while hydrogen bond/electrostatic interactions were observed between the carboxylic group of elafibranor and Ser280/Tyr314/His440/Tyr464 in PPAR α -LBD (Figure 6C). Regrettably, we failed to obtain PPAR δ/γ -LBD–elafibranor cocrystals (Figure S1H,I), although elafibranor did activate PPAR δ/γ to some extent (Figures 1D and 2E,F).

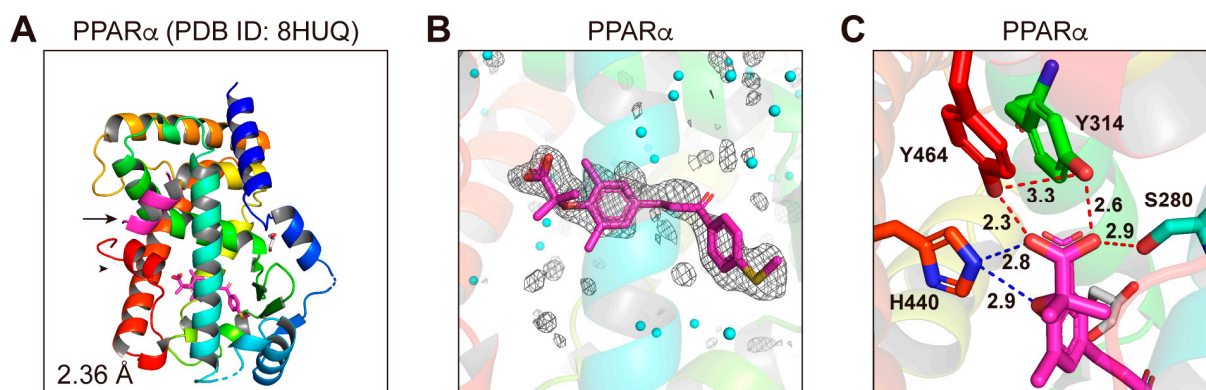


Figure 6. PPAR α -LBD–elafibranor cocrystal structures. A cocrystal of elafibranor and PPAR α -LBD (A–C) was analyzed using X-ray diffraction. (A) The 2.36 Å resolution overall structure of the complex deposited in PDB ID: 8HUQ. The SRC1 peptide (α -helix in magenta) and the AF-2 helix 12 (α -helix in red) are indicated by an arrow and an arrowhead, respectively. (B) Magnified view of elafibranor located in the “Center” and the “Arm II” regions of PPAR α -LBD. The electron density is shown in the mesh via F_o-F_c omit maps contoured at $+3.0\sigma$. Water molecules are presented as cyan spheres. (C) Hydrogen bonds and electrostatic interactions between elafibranor and the four consensus amino acid residues (that recognize the carboxyl moiety of elafibranor) are indicated by red and blue dotted lines, respectively, along with their distances (in Å).

3.7. LBP Regional Localization of the Five PPAR Ligands in PPAR $\alpha/\delta/\gamma$ -LBD

PPAR $\alpha/\delta/\gamma$ -LBP comprises five regions (Figure 7A) [14,15,17]. In PPAR α -LBP, seladelpar, elafibranor, and saroglitazar (PDB ID: 6LXB/6LXC using different crystallization methods) [15] were located in the “Center” and in the “Arm II/X” regions, whereas lanifibranor was only found in the “Center” (Figure 7B). In PPAR δ -LBP, lanifibranor was located in the “Center,” and seladelpar was located in the “Center” and the “Arm II” regions (Figure 7C). In PPAR γ -LBP, lanifibranor was only found in the “Center” while seladelpar and saroglitazar (PDB ID: 7E0A) [17] were found in the “Center” and the “Arm II/X”

regions. Mueller et al. deposited a PPAR γ -LBD–pioglitazone structure in the PDB, in which two pioglitazone molecules were located in LBP (PDB ID: 2XKW; not published in a paper): one was in the “Center” and the “Arms II/X” regions and the other was in the “Arms II/III” (Figure 7D). These results indicate that each PPAR ligand has a flexible molecular frame allowing it to bind to different regions of the PPAR $\alpha/\delta/\gamma$ -LBPs.

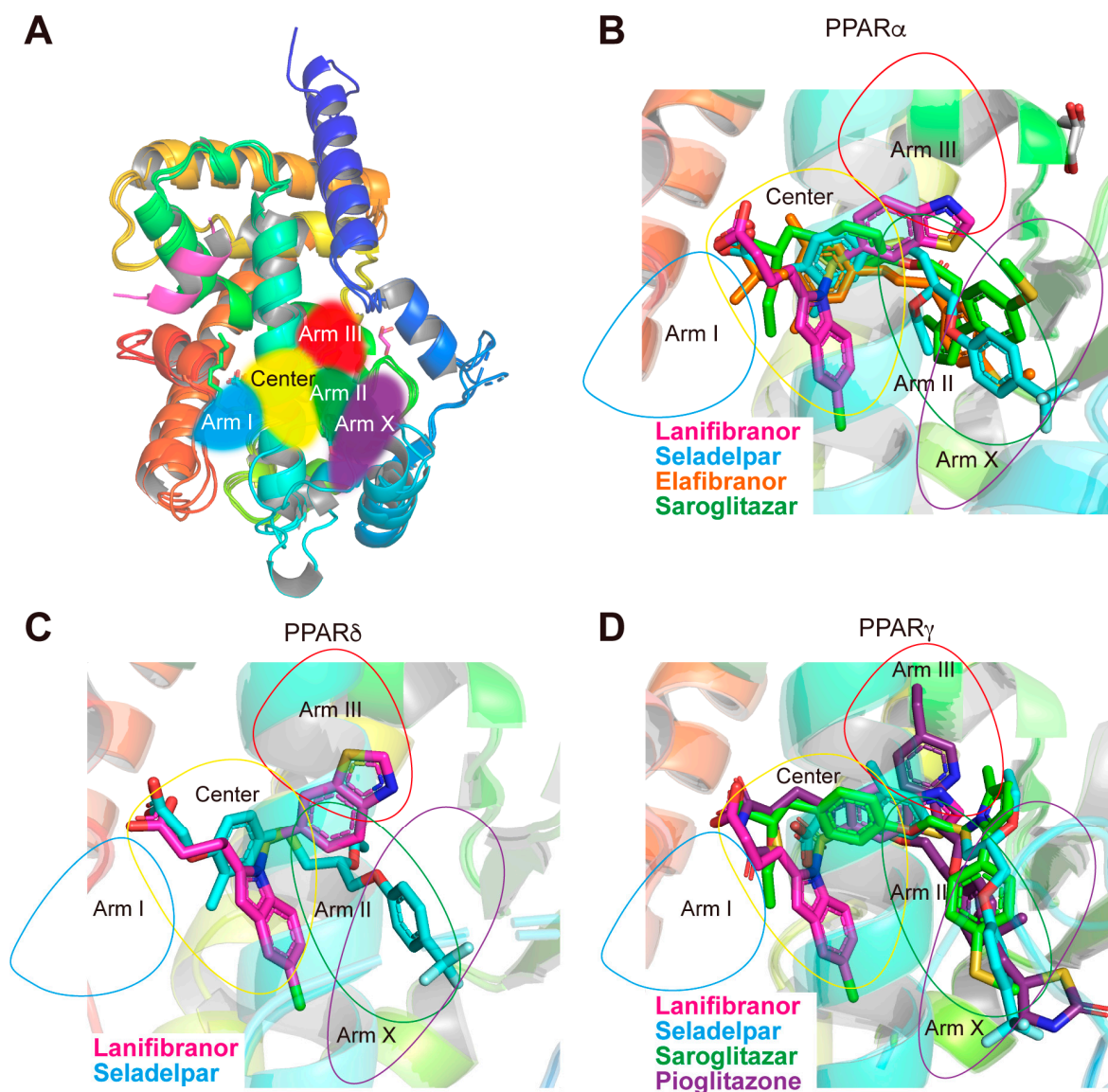


Figure 7. Ligand-binding pocket (LBP) regional localization of five PPAR ligands in PPAR $\alpha/\delta/\gamma$ -LBD. (A) LBP comprising the “Center” and the “Arms I–III and X” regions of PPAR $\alpha/\delta/\gamma$ -LBD [15]. (B) Superimposed image of lanifibranor (magenta; from 8HUK), seladelpar (cyan; 8HUN), elafibranor (orange; 8HUQ), and saroglitazar (green; 6LXC) [15] in PPAR α -LBD. (C) Superimposed image of lanifibranor (magenta; 8HUL) and seladelpar (cyan; 8HUO) in PPAR δ -LBD. (D) Superimposed image of lanifibranor (magenta; 8HUM), seladelpar (cyan; 8HUP), saroglitazar (green; 7E0A) [17], and pioglitazone (purple; 2XKW) in PPAR γ -LBD.

3.8. Molecular Interactions between PPAR $\alpha/\delta/\gamma$ -LBD Amino Acids and the Ligands

For more detailed comparisons of ligand binding loci, proximity distances (≤ 4.5 Å) between each amino acid in PPAR $\alpha/\delta/\gamma$ -LBD and the ligands (lanifibranor, seladelpar, and elafibranor) were measured using PyMOL, and the MolDock scores (a kind of binding potential) of their interactions were calculated (Table S2). The four consensus amino

acids surrounding the carboxylic groups of the ligands were stabilized by ligand binding (as manifested by minus MolDock scores), except for PPAR γ -LBD–seladelpar, in which hydrogen bonds were not formed between His323/Tyr473 and the ligand (Figure 5I). Some other consensus amino acids, such as Ile272/Cys276/Phe318/Leu321 in PPAR α -LBD, Val245/Cys249/Phe291/Leu294 in PPAR δ -LBD, and Ile281/Cys285/Tyr327/Leu330 in PPAR γ -LBD, were stabilized by all three ligands, whereas some consensus amino acids (i.e., Leu247/Ala250/Val255/Ala333 in PPAR α -LBD and Leu255/Glu259/Phe264/Ser342 in PPAR γ -LBD) were specifically stabilized by seladelpar and other consensus amino acids (i.e., Leu347/Phe351, Leu320/Phe324 and Leu356/Phe360 in PPAR $\alpha/\delta/\gamma$ -LBD, respectively) were stabilized only by lanifibranor (Table S2).

4. Discussion

This study investigated how lanifibranor, seladelpar, and elafibranor bind to and activate PPAR $\alpha/\delta/\gamma$ subtypes. Major antioxidant genes, including catalase, heme oxygenase-1, glutathione peroxidase 3/4, superoxide dismutase 2/3, thioredoxin, CD36, and uncoupling protein 2/3, contain PPAR responsive element (PPRE) in their promoter regions and are transcriptionally regulated by the PPARs [34–36]. In addition, a putative PPRE is present in the promoter region of Nrf2 that is one of the most important regulators of cellular responses to oxidative stress and inflammation [37]. Therefore, such PPAR agonists might potentially modulate systemic redox homeostasis and inflammation as well as lipid/insulin signaling to counteract NASH.

Lanifibranor, the PPAR $\alpha/\delta/\gamma$ pan agonist developed by Inventiva (Daix, France) [31], was first described for its prevention of experimental skin [38] and lung fibrosis [39], and was then applied to liver fibrosis [40]. In a phase 2b study involving 247 patients with active NASH (NCT03008070), lanifibranor significantly improved general NASH conditions [41]. A large-scale (~1000 patients) phase 3 study, evaluating the long-term efficacy and safety of lanifibranor in adult NASH patients with Fibrosis 2/3 stage of liver fibrosis (NCT04849728) is currently underway, and its results have not been posted yet. The EC₅₀ values for PPAR $\alpha/\delta/\gamma$ were in small ranges (0.4–5 μ M in Figure 1B and 3–14 μ M in Figure 2A,B), and therefore, lanifibranor in clinical doses seems to be able to activate all PPAR subtypes at once. Due to the fact that its efficacies for PPAR γ activation often match with those of pioglitazone (Figure 2A vs. Figure 2I, Figure 2B vs. Figure 2J), and Figure 3B vs. Figure 3F), PPAR γ -related undesirable side effects (such as weight gain, edema, bone loss, and congestive heart failure) [42] should be closely monitored in the case of lanifibranor. In the cocrystal structures, indeglitazar, another PPAR $\alpha/\delta/\gamma$ pan agonist that resembles lanifibranor in structure, has also been reported to exist in the similar “Center” regions in PPAR $\alpha/\delta/\gamma$ (PDB ID: 3ET1, 3ET2, and 3ET3, respectively) [43] and some consensus amino acids in the Center region (such as Phe273/Ile354, Phe246/Ile327, and Phe282/Phe363 in PPAR $\alpha/\delta/\gamma$ -LBD, respectively) were highly stabilized by lanifibranor (Table S2); therefore, such molecular frames might be favorable for a PPAR pan activity.

Seladelpar is the novel PPAR δ -selective agonist developed by CymaBay Therapeutics (Newark, NJ, USA) [44]. Although its clinical trial against NAFLD/NASH was once discontinued at phase 2 due to abnormal findings on liver biopsy [9], the FDA thereafter lifted the injunction on July 2020 due to subsequent doubts about the relevance of the drug [45]. The clinical trials have not resumed since then, and thus, its therapeutic potential against NASH remains unknown. In its clinical trial against hyperlipidemia (NCT00701883), seladelpar reduced the assessed blood lipid parameters (triglyceride, total cholesterol, LDL-cholesterol, and free fatty acid levels), the alkaline phosphatase and γ -glutamyl transferase (GGT) activities, and the homeostatic model assessment–insulin resistance [46]. Moreover, prompted by its positive results in its phase 2 clinical trial for primary biliary cholangitis, a phase 3 clinical trial is currently underway [44,47]. In mice, seladelpar has been reported to reverse dyslipidemia and the hepatic storage of lipotoxic lipids, thereby improving the NASH pathology in atherogenic-diet-fed obese diabetic mice [48]. Seladelpar could activate all PPAR subtypes; however, the EC₅₀ values for PPAR δ -LBD were ~2 orders lower

than those for PPAR α/γ -LBD (Figures 1C and 2C,D), and this is why seladelpar can be used as a PPAR δ -selective agonist in clinical use. In the cocrystal structures, seladelpar was bound to the “Center” and the “Arm II” regions of all PPAR $\alpha/\delta/\gamma$ -LBDs (Figure 5J), similar to the PPAR δ -selective full agonist GW501516 in PPAR δ -LBD (PDB ID: 5U46) [49]. Both carboxylic and trifluoromethyl groups of seladelpar were located in positions similar to those of GW501516, thereby implying that amino acid residues in those regions were important for the full activation of PPAR δ . Indeed, Val298, Leu303, Val312, and Ile328, which were reported to be important for the binding to GW501516 and other synthetic PPAR δ -selective ligands [49], were all stabilized by seladelpar (Table S2).

Elafibranor, the PPAR α/δ dual agonist developed by Genfit (Loos, France), has been abandoned at the phase 3 clinical trial against NAFLD/NASH due to its non-significant effect on the primary endpoint of the resolution of NASH without a worsening of fibrosis [10]. In a phase 2 clinical trial (NCT01694849), its efficacy and safety at 80 and 120 mg/day doses for 52 weeks were confirmed among the 275 participating NASH patients [50]. Elafibranor also reduced the fasting plasma triglyceride levels and GGT activities, increased HDL cholesterol, and decreased insulin resistance and fasting plasma glucose levels, in abdominally obese patients with either combined dyslipidemia or prediabetes [51]. Further clinical trials have suggested that elafibranor can improve peripheral and hepatic insulin sensitivity [52]. As its EC₅₀ values for PPAR $\alpha/\delta/\gamma$ -LBD were in small ranges (0.4–3 μ M in Figure 1D and 5–16 μ M in Figure 2E,F), elafibranor in clinical doses seems to be able to activate all PPAR subtypes at once. The efficacy of elafibranor for PPAR γ activation was lower than that of pioglitazone in the cases of transactivation (Figure 1D,F), PGC1 α (Figure 2E,I), and SRC1 recruitment (Figure 2F,J). Interestingly, the impact of elafibranor on the thermal stability of PPAR $\alpha/\delta/\gamma$ -LBD was much weaker than that of other ligands (Figure 3D). Regrettably, we failed to obtain PPAR δ/γ -LBD–elafibranor cocrystals (Figure S1H,I). Therefore, it might be difficult for elafibranor to form stable complexes with any of the PPAR subtypes, especially with PPAR δ/γ , and to induce enough clinical impact in some cases (e.g., NASH).

When compared to the LBPs of other nuclear receptors that have 600–1100 \AA^3 cavities, the LBPs of PPAR $\alpha/\delta/\gamma$ have relatively large (1300–1440 \AA^3) cavities that are able to accept 1–4 ligand molecules [15]. The PPAR $\alpha/\delta/\gamma$ -LBD–various ligands’ cocrystal structures registered in the PDB until 18 July 2023 (60, 52, and 288, respectively; among which 40, 8, and 25 registrations, respectively, derive from our laboratories) demonstrate their extremely diverse ligand binding modes. We have, herein, added seven novel structures (three, two, and two for PPAR $\alpha/\delta/\gamma$, respectively) with altered ligand locations. However, unfortunately, we failed to provide a clear molecular basis (such as close interactions with specific PPAR-LBD amino acids; Table S2) for PPAR $\alpha/\delta/\gamma$ targeting preferences of these three drugs, perhaps in part for large PPAR-LBPs, which is the limitation of this study. Nevertheless, future drug discovery for NASH will undoubtedly benefit from functional and structural investigation of the PPAR $\alpha/\delta/\gamma$ -ligand molecular interactions such as in this study. Lanifibranor (rather than elafibranor) could be a prototype of PPAR pan agonists that bind to the similar positions in PPAR $\alpha/\delta/\gamma$ -LBD and thus have comparable preferences for PPAR $\alpha/\delta/\gamma$, and seladelpar could be a lead compound of upcoming PPAR δ -selective agonists with more preferences to PPAR δ and less preferences to PPAR α/γ .

Supplementary Materials: The following supporting information can be downloaded at: <https://www.mdpi.com/article/10.3390/antiox12081523/s1>, Figure S1: Snapshots of the crystals as mounted on the BL5A or BL17A beamline goniometers; Figure S2: Other subunit structures of PPAR α/δ dimers in the cocrystals; Table S1: Data collection and refinement statistics (molecular replacement); Table S2 (A separate Excel file): All PPAR $\alpha/\delta/\gamma$ -LBD amino acids that have ≤ 4.5 \AA proximity distances from lanifibranor, seladelpar, and elafibranor, and the MolDock scores of their molecular interactions.

Author Contributions: Conceptualization, validation, formal analysis, data curation, writing—original draft preparation, visualization, S.K., A.H. and I.I.; methodology, resources, writing—review and editing, S.K., A.H., T.O. and I.I.; investigation, S.K., A.H., R.I., M.A., A.F., C.K., S.M., Y.H., Y.S.,

K.U., Y.M., T.O. and I.I.; supervision, project administration, I.I.; funding acquisition, S.K., T.O. and I.I. All authors have read and agreed to the published version of the manuscript.

Funding: This work was funded in part by the Platform Project for Supporting Drug Discovery and Life Science Research (Basis for Supporting Innovative Drug Discovery and Life Science Research (BINDS)) from AMED (grant number: JP21am0101071; support number: 1407 (S.K. and I.I.)), a Grant-in-Aid for Early Career Scientists from MEXT (22K15049 to S.K.), a Grant-in-Aid for Transformative Research Areas (A) (22H05577 to I.I.) from JSPS, and Terumo Life Science Foundation (to T.O.). This work was performed under the approval of the Photon Factory Program Advisory Committee (proposal numbers: 2018G658/2022G663). A.H. is supported by a scholarship from the Chugai Foundation for Innovative Drug Discovery Science (2021–2022) and Nagai Memorial Research Scholarship from the Pharmaceutical Society of Japan (2022–2024).

Institutional Review Board Statement: Not applicable.

Informed Consent Statement: Not applicable.

Data Availability Statement: The X-ray diffraction datasets have been deposited in the PDB with accession numbers: 8HUK, 8HUL, 8HUM, 8HUN, 8HUO, 8HUP, and 8HUQ.

Conflicts of Interest: The authors declare no conflict of interest.

References

1. Chalasani, N.; Younossi, Z.; Lavine, J.E.; Charlton, M.; Cusi, K.; Rinella, M.; Harrison, S.A.; Brunt, E.M.; Sanyal, A.J. The diagnosis and management of nonalcoholic fatty liver disease: Practice guidance from the American Association for the Study of Liver Diseases. *Hepatology* **2018**, *67*, 328–357. [[CrossRef](#)]
2. Riazi, K.; Azhari, H.; Charette, J.H.; Underwood, F.E.; King, J.A.; Afshar, E.E.; Swain, M.G.; Congly, S.E.; Kaplan, G.G.; Shaheen, A.A. The prevalence and incidence of NAFLD worldwide: A systematic review and meta-analysis. *Lancet Gastroenterol. Hepatol.* **2022**, *7*, 851–861. [[CrossRef](#)]
3. Ma, Y.; Lee, G.; Heo, S.Y.; Roh, Y.S. Oxidative stress is a key modulator in the development of nonalcoholic fatty liver disease. *Antioxidants* **2021**, *11*, 91. [[CrossRef](#)]
4. Sheka, A.C.; Adeyi, O.; Thompson, J.; Hameed, B.; Crawford, P.A.; Ikramuddin, S. Nonalcoholic steatohepatitis: A review. *JAMA* **2020**, *323*, 1175–1183. [[CrossRef](#)]
5. Vuppalanchi, R.; Noureddin, M.; Alkhoury, N.; Sanyal, A.J. Therapeutic pipeline in nonalcoholic steatohepatitis. *Nat. Rev. Gastroenterol. Hepatol.* **2021**, *18*, 373–392. [[CrossRef](#)]
6. Friedman, S.L.; Neuschwander-Tetri, B.A.; Rinella, M.; Sanyal, A.J. Mechanisms of NAFLD development and therapeutic strategies. *Nat. Med.* **2018**, *24*, 908–922. [[CrossRef](#)]
7. Francque, S.; Szabo, G.; Abdelmalek, M.F.; Byrne, C.D.; Cusi, K.; Dufour, J.F.; Roden, M.; Sacks, F.; Tacke, F. Nonalcoholic steatohepatitis: The role of peroxisome proliferator-activated receptors. *Nat. Rev. Gastroenterol. Hepatol.* **2021**, *18*, 24–39. [[CrossRef](#)]
8. Cheng, H.S.; Tan, W.R.; Low, Z.S.; Marvalim, C.; Lee, J.Y.H.; Tan, N.S. Exploration and development of PPAR modulators in health and disease: An update of clinical evidence. *Int. J. Mol. Sci.* **2019**, *20*, 5055. [[CrossRef](#)]
9. CymaBay Therapeutics Press Release. CymaBay Therapeutics Halts Clinical Development of Seladelpar. 25 November 2019. Available online: <https://ir.cymabay.com/press-releases/detail/476/cymabay-therapeutics-halts-clinical-development-of-seladelpar> (accessed on 22 June 2023).
10. GENFIT Press Release (11 May 2020). GENFIT: Announces Results from Interim Analysis of RESOLVE-IT Phase 3 Trial of Elafibranor in Adults with NASH and Fibrosis. Available online: <https://ir.genfit.com/news-releases/news-release-details/genfit-announces-results-interim-analysis-resolve-it-phase-3/> (accessed on 22 June 2023).
11. Lehmann, J.M.; Moore, L.B.; Smith-Oliver, T.A.; Wilkison, W.O.; Willson, T.M.; Kliewer, S.A. An antidiabetic thiazolidinedione is a high affinity ligand for peroxisome proliferator-activated receptor gamma (PPAR gamma). *J. Biol. Chem.* **1995**, *270*, 12953–12956. [[CrossRef](#)]
12. Itoh, T.; Fairall, L.; Amin, K.; Inaba, Y.; Szanto, A.; Balint, B.L.; Nagy, L.; Yamamoto, K.; Schwabe, J.W. Structural basis for the activation of PPARgamma by oxidized fatty acids. *Nat. Struct. Mol. Biol.* **2008**, *15*, 924–931. [[CrossRef](#)]
13. Kang, T.; Martins, T.; Sadowski, I. Wild type GAL4 binds cooperatively to the GAL1-10 UASG in vitro. *J. Biol. Chem.* **1993**, *268*, 9629–9635. [[CrossRef](#)] [[PubMed](#)]
14. Honda, A.; Kamata, S.; Akahane, M.; Machida, Y.; Uchii, K.; Shiiyama, Y.; Habu, Y.; Miyawaki, S.; Kaneko, C.; Oyama, T.; et al. Functional and structural insights into human PPAR $\alpha/\delta/\gamma$ subtype selectivity of bezafibrate, fenofibric acid, and pemafibrate. *Int. J. Mol. Sci.* **2022**, *23*, 4726. [[CrossRef](#)]
15. Kamata, S.; Oyama, T.; Saito, K.; Honda, A.; Yamamoto, Y.; Suda, K.; Ishikawa, R.; Itoh, T.; Watanabe, Y.; Shibata, T.; et al. PPAR α ligand-binding domain structures with endogenous fatty acids and fibrates. *iScience* **2020**, *23*, 101727. [[CrossRef](#)]

16. Kamata, S.; Oyama, T.; Ishii, I. Preparation of co-crystals of human PPAR α -LBD and ligand for high-resolution X-ray crystallography. *STAR Protoc.* **2021**, *2*, 100364. [[CrossRef](#)] [[PubMed](#)]
17. Honda, A.; Kamata, S.; Satta, C.; Machida, Y.; Uchii, K.; Terasawa, K.; Nemoto, A.; Oyama, T.; Ishii, I. Structural basis for anti-non-alcoholic fatty liver disease and diabetic dyslipidemia drug saroglitazar as a PPAR α/γ dual agonist. *Biol. Pharm. Bull.* **2021**, *44*, 1210–1219. [[CrossRef](#)] [[PubMed](#)]
18. Kelly, S.M.; Jess, T.J.; Price, N.C. How to study proteins by circular dichroism. *Biochim. Biophys. Acta* **2005**, *1751*, 119–139. [[CrossRef](#)] [[PubMed](#)]
19. Kabsch, W. XDS. *Acta Crystallogr. D Biol. Crystallogr.* **2010**, *66*, 125–132. [[CrossRef](#)]
20. Evans, P.R.; Murshudov, G.N. How good are my data and what is the resolution? *Acta Crystallogr. D Biol. Crystallogr.* **2013**, *69*, 1204–1214. [[CrossRef](#)]
21. McCoy, A.J.; Grosse-Kunstleve, R.W.; Adams, P.D.; Winn, M.D.; Storoni, L.C.; Read, R.J. Phaser crystallographic software. *J. Appl. Crystallogr.* **2007**, *40*, 658–674. [[CrossRef](#)]
22. Emsley, P.; Cowtan, K. Coot: Model-building tools for molecular graphics. *Acta Crystallogr. D Biol. Crystallogr.* **2004**, *60*, 2126–2132. [[CrossRef](#)]
23. Adams, P.D.; Afonine, P.V.; Bunkóczi, G.; Chen, V.B.; Davis, I.W.; Echols, N.; Headd, J.J.; Hung, L.W.; Kapral, G.J.; Grosse-Kunstleve, R.W.; et al. PHENIX: A comprehensive Python-based system for macromolecular structure solution. *Acta Crystallogr. D Biol. Crystallogr.* **2010**, *66*, 213–221. [[CrossRef](#)] [[PubMed](#)]
24. Yu, S.; Reddy, J.K. Transcription coactivators for peroxisome proliferator-activated receptors. *Biochim. Biophys. Acta* **2007**, *1771*, 936–951. [[CrossRef](#)] [[PubMed](#)]
25. Feige, J.N.; Auwerx, J. Transcriptional coregulators in the control of energy homeostasis. *Trends Cell Biol.* **2007**, *17*, 292–301. [[CrossRef](#)] [[PubMed](#)]
26. Mouchiroud, L.; Eichner, L.J.; Shaw, R.J.; Auwerx, J. Transcriptional coregulators: Fine-tuning metabolism. *Cell Metab.* **2014**, *20*, 26–40. [[CrossRef](#)]
27. Lefere, S.; Puengel, T.; Hundertmark, J.; Penners, C.; Frank, A.K.; Guillot, A.; de Muynck, K.; Heymann, F.; Adarbes, V.; Defrène, E.; et al. Differential effects of selective- and pan-PPAR agonists on experimental steatohepatitis and hepatic macrophages. *J. Hepatol.* **2020**, *73*, 757–770. [[CrossRef](#)] [[PubMed](#)]
28. Kouno, T.; Liu, X.; Zhao, H.; Kisseleva, T.; Cable, E.E.; Schnabl, B. Selective PPAR δ agonist seladelpar suppresses bile acid synthesis by reducing hepatocyte CYP7A1 via the fibroblast growth factor 21 signaling pathway. *J. Biol. Chem.* **2022**, *298*, 102056. [[CrossRef](#)]
29. Schattenberg, J.M.; Pares, A.; Kowdley, K.V.; Heneghan, M.A.; Caldwell, S.; Pratt, D.; Bonder, A.; Hirschfield, G.M.; Levy, C.; Vierling, J.; et al. A randomized placebo-controlled trial of elafibranor in patients with primary biliary cholangitis and incomplete response to UDCA. *J. Hepatol.* **2021**, *74*, 1344–1354. [[CrossRef](#)]
30. Afzal, S.; Sattar, M.A.; Johns, E.J.; Eseyin, O.A. Peroxisome proliferator-activated receptor agonist (pioglitazone) with exogenous adiponectin ameliorates arterial stiffness and oxidative stress in diabetic Wistar Kyoto rats. *Eur. J. Pharmacol.* **2021**, *907*, 174218. [[CrossRef](#)] [[PubMed](#)]
31. Boubia, B.; Poupardin, O.; Barth, M.; Binet, J.; Peralba, P.; Mounier, L.; Jacquier, E.; Gauthier, E.; Lepais, V.; Chatar, M.; et al. Design, synthesis, and evaluation of a novel series of indole sulfonamide peroxisome proliferator activated receptor (PPAR) $\alpha/\gamma/\delta$ triple activators: Discovery of lanifibranor, a new antifibrotic clinical candidate. *J. Med. Chem.* **2018**, *61*, 2246–2265. [[CrossRef](#)]
32. Yang, Z.; Muccio, D.D.; Melo, N.; Atigadda, V.R.; Renfrow, M.B. Stability of the retinoid X receptor- α homodimer in the presence and absence of retinoid and coactivator peptide. *Biochemistry* **2021**, *60*, 1165–1177. [[CrossRef](#)]
33. Yu, C.; Chen, L.; Luo, H.; Chen, J.; Cheng, F.; Gui, C.; Zhang, R.; Shen, J.; Chen, K.; Jiang, H.; et al. Binding analyses between human PPAR γ -LBD and ligands. *Eur. J. Biochem.* **2004**, *271*, 386–397. [[CrossRef](#)] [[PubMed](#)]
34. Muzio, G.; Barrera, G.; Pizzimenti, S. Peroxisome proliferator-activated receptors (PPARs) and oxidative stress in physiological conditions and in cancer. *Antioxidants* **2021**, *10*, 1734. [[CrossRef](#)] [[PubMed](#)]
35. Miao, M.; Wang, X.; Liu, T.; Li, Y.J.; Yu, W.Q.; Yang, T.M.; Guo, S.D. Targeting PPARs for therapy of atherosclerosis: A review. *Int. J. Biol. Macromol.* **2023**, *242*, 125008. [[CrossRef](#)] [[PubMed](#)]
36. Chen, H.; Tan, H.; Wan, J.; Zeng, Y.; Wang, J.; Wang, H.; Lu, X. PPAR- γ signaling in nonalcoholic fatty liver disease: Pathogenesis and therapeutic targets. *Pharmacol. Ther.* **2023**, *245*, 108391. [[CrossRef](#)]
37. Park, E.Y.; Cho, I.J.; Kim, S.G. Transactivation of the PPAR-responsive enhancer module in chemopreventive glutathione S-transferase gene by the peroxisome proliferator-activated receptor- γ and retinoid X receptor heterodimer. *Cancer Res.* **2004**, *64*, 3701–3713. [[CrossRef](#)]
38. Ruzehaji, N.; Frantz, C.; Ponsoye, M.; Avouac, J.; Pezet, S.; Guilbert, T.; Luccarini, J.M.; Broqua, P.; Junien, J.L.; Allanore, Y. Pan PPAR agonist IVA337 is effective in prevention and treatment of experimental skin fibrosis. *Ann. Rheum. Dis.* **2016**, *75*, 2175–2183. [[CrossRef](#)]
39. Avouac, J.; Konstantinova, I.; Guignabert, C.; Pezet, S.; Sadoine, J.; Guilbert, T.; Cauvet, A.; Tu, L.; Luccarini, J.M.; Junien, J.L.; et al. Pan-PPAR agonist IVA337 is effective in experimental lung fibrosis and pulmonary hypertension. *Ann. Rheum. Dis.* **2017**, *76*, 1931–1940. [[CrossRef](#)]

40. Boyer-Diaz, Z.; Aristu-Zabalza, P.; Andrés-Rozas, M.; Robert, C.; Ortega-Ribera, M.; Fernández-Iglesias, A.; Broqua, P.; Junien, J.L.; Wettstein, G.; Bosch, J.; et al. Pan-PPAR agonist lanifibranor improves portal hypertension and hepatic fibrosis in experimental advanced chronic liver disease. *J. Hepatol.* **2021**, *74*, 1188–1199. [[CrossRef](#)]
41. Francque, S.M.; Bedossa, P.; Ratziu, V.; Anstee, Q.M.; Bugianesi, E.; Sanyal, A.J.; Loomba, R.; Harrison, S.A.; Balabanska, R.; Mateva, L.; et al. A randomized, controlled trial of the pan-PPAR agonist lanifibranor in NASH. *N. Engl. J. Med.* **2021**, *385*, 1547–1558. [[CrossRef](#)]
42. Wang, S.; Dougherty, E.J.; Danner, R.L. PPAR γ signaling and emerging opportunities for improved therapeutics. *Pharmacol. Res.* **2016**, *111*, 76–85. [[CrossRef](#)]
43. Artis, D.R.; Lin, J.J.; Zhang, C.; Wang, W.; Mehra, U.; Perreault, M.; Erbe, D.; Krupka, H.I.; England, B.P.; Arnold, J.; et al. Scaffold-based discovery of indeglitazar, a PPAR pan-active anti-diabetic agent. *Proc. Natl. Acad. Sci. USA* **2009**, *106*, 262–267. [[CrossRef](#)]
44. Bowlus, C.L.; Galambos, M.R.; Aspinall, R.J.; Hirschfield, G.M.; Jones, D.E.J.; Dörffel, Y.; Gordon, S.C.; Harrison, S.A.; Kremer, A.E.; Mayo, M.J.; et al. A phase II, randomized, open-label, 52-week study of seladelpar in patients with primary biliary cholangitis. *J. Hepatol.* **2022**, *77*, 353–364. [[CrossRef](#)]
45. CymaBay Therapeutics Press Release. FDA Lifts all Clinical Holds on Seladelpar. 23 July 2020. Available online: <https://ir.cymabay.com/press-releases/detail/485/fda-lifts-all-clinical-holds-on-seladelpar> (accessed on 22 June 2023).
46. Bays, H.E.; Schwartz, S.; Littlejohn, T., 3rd; Kerzner, B.; Krauss, R.M.; Karpf, D.B.; Choi, Y.J.; Wang, X.; Naim, S.; Roberts, B.K. MBX-8025, a novel peroxisome proliferator receptor-delta agonist: Lipid and other metabolic effects in dyslipidemic overweight patients treated with and without atorvastatin. *J. Clin. Endocrinol. Metab.* **2011**, *96*, 2889–2897. [[CrossRef](#)] [[PubMed](#)]
47. Kremer, A.E.; Mayo, M.J.; Hirschfield, G.; Levy, C.; Bowlus, C.L.; Jones, D.E.; Steinberg, A.; McWherter, C.A.; Choi, Y.J. Seladelpar improved measures of pruritus, sleep, and fatigue and decreased serum bile acids in patients with primary biliary cholangitis. *Liver Int.* **2022**, *42*, 112–123. [[CrossRef](#)] [[PubMed](#)]
48. Haczejni, F.; Wang, H.; Barn, V.; Mridha, A.R.; Yeh, M.M.; Haigh, W.G.; Ioannou, G.N.; Choi, Y.J.; McWherter, C.A.; Teoh, N.C.; et al. The selective peroxisome proliferator-activated receptor-delta agonist seladelpar reverses nonalcoholic steatohepatitis pathology by abrogating lipotoxicity in diabetic obese mice. *Hepatol. Commun.* **2017**, *1*, 663–674. [[CrossRef](#)]
49. Wu, C.C.; Baiga, T.J.; Downes, M.; La Clair, J.J.; Atkins, A.R.; Richard, S.B.; Fan, W.; Stockley-Noel, T.A.; Bowman, M.E.; Noel, J.P.; et al. Structural basis for specific ligation of the peroxisome proliferator-activated receptor δ . *Proc. Natl. Acad. Sci. USA* **2017**, *114*, E2563–E2570. [[CrossRef](#)] [[PubMed](#)]
50. Ratziu, V.; Harrison, S.A.; Francque, S.; Bedossa, P.; Lehert, P.; Serfaty, L.; Romero-Gomez, M.; Boursier, J.; Abdelmalek, M.; Caldwell, S.; et al. Elafibranor, an agonist of the peroxisome proliferator-activated receptor- α and - δ , induces resolution of nonalcoholic steatohepatitis without fibrosis worsening. *Gastroenterology* **2016**, *150*, 1147–1159.e1145. [[CrossRef](#)] [[PubMed](#)]
51. Cariou, B.; Zaïr, Y.; Staels, B.; Bruckert, E. Effects of the new dual PPAR α/δ agonist GFT505 on lipid and glucose homeostasis in abdominally obese patients with combined dyslipidemia or impaired glucose metabolism. *Diabetes Care* **2011**, *34*, 2008–2014. [[CrossRef](#)]
52. Cariou, B.; Hanf, R.; Lambert-Porcheron, S.; Zaïr, Y.; Sauvinet, V.; Noël, B.; Flet, L.; Vidal, H.; Staels, B.; Laville, M. Dual peroxisome proliferator-activated receptor α/δ agonist GFT505 improves hepatic and peripheral insulin sensitivity in abdominally obese subjects. *Diabetes Care* **2013**, *36*, 2923–2930. [[CrossRef](#)]

Disclaimer/Publisher’s Note: The statements, opinions and data contained in all publications are solely those of the individual author(s) and contributor(s) and not of MDPI and/or the editor(s). MDPI and/or the editor(s) disclaim responsibility for any injury to people or property resulting from any ideas, methods, instructions or products referred to in the content.